



# Design and analysis of different horn profiles using FEM for vibration assisted machining

Gamidi Kartheek<sup>1</sup> · Pasam Vamsi Krishna<sup>1</sup>

Received: 15 August 2021 / Accepted: 18 November 2021 / Published online: 8 December 2021  
© The Author(s), under exclusive licence to Springer Nature Switzerland AG 2021

## Abstract

Ultrasonic machining is one of the hybrid machining processes which is gaining importance in the manufacturing of hard to cut materials particularly aerospace alloys. The success of ultrasonic machining will depend on the applied vibration parameters, viz. amplitude and frequency. In ultrasonic machining setup, the vibrations from the transducer are amplified and concentrated at desired location by the horn. The increment in amplitude reduces the tool work contact ratio (TWCR) and vice versa. Surface roughness, cutting forces, cutting temperatures and tool wear are affected by TWCR. Higher amplitude will reduce the TWCR and enhances the machining performance. Hence, proper design of the horn will enhance the amplification and therefore the machining efficiency. In this work, the influence of horn diameter ratio, horn profile, and length variation within the horn on deformation, amplification and effective stress are studied. Titanium is chosen as horn material. Horns of single exponential, double exponential and mixed horn profiles are studied through modeling and simulation using Finite Element Analysis (FEA). The tool end diameter of the horns is varied from 10 to 20 mm in steps of 2.5 mm for all the horn profiles. Further, double exponential and mixed horns are modeled and analyzed with three length variations in each case. All these are subjected to longitudinal vibrations along the axial direction with same amplitude and frequency. The analysis revealed that horns with lower diameter ratio are yielding high amplification. In addition, horns with double exponential profile with 5050 length variation and 10-mm tool end diameter, mixed horn with 2575 length variation and 10-mm tool end diameter are proved as best designs. The high amplification of horns at lower tool end diameters is attributed to their reduced strength because of reduced cross section. The stress concentration because of abrupt change in the cross section in case of double exponential and mixed horns also contributed to increase in effective stress.

**Keywords** Horn design · UVAM · Amplification · Harmonic analysis · Single exponential horn · Double exponential horn · Mixed profile horns

## 1 Introduction

Ultrasonic machining is an advanced machining process finding its application particularly in machining of difficult to cut materials like Titanium and Nickel alloys. Since these metals are most consumed materials in aerospace industry, it is obvious that ultrasonic machining is fitting technology for the same. The use of ultrasonic energy, i.e., amplitude and frequency of vibrations, for enhancing a machining performance is the principle behind ultrasonic machining. The components of any ultrasonic machining process can be iden-

tified from the schematic shown in Fig. 1. It consists of a generator, transducer and sonotrode (booster and horn). The ultrasonic vibrations are generated by the piezoelectric transducer with a high frequency (20–40 kHz) and low amplitude (3–4 microns). However the frequency usually adopted is 20 kHz. The success in the application of ultrasonic machining lies in its amplitude. A booster is used for amplifying the amplitude (up to 15 microns). This gets further amplified by a horn or concentrator (20–100 microns) which also acts as a carrier of ultrasonic energy to the tool. The tool attached at the free end of the horn will vibrate in the respective direction performing the cutting process.

A lot of research is reported in the literature emphasizing the use of ultrasonic energy in machining. Ultrasonic assisted machining (UAM) process with axial vibrations was designed and developed in investigating the effect of process

✉ Gamidi Kartheek  
gkartheek041@gmail.com

<sup>1</sup> Department of Mechanical Engineering, National Institute of Technology Warangal, Warangal, Telangana 506004, India

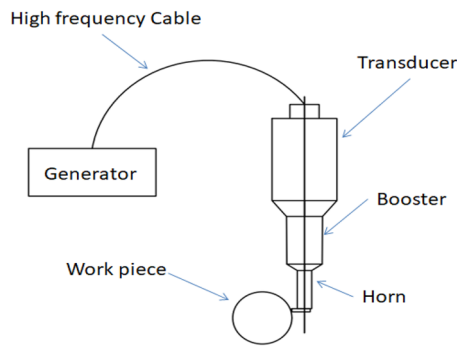


**Fig. 1** Schematic of ultrasonic machining setup (Turning)

parameters on cutting forces by Verma and Pandey (2019). Al6063 aluminium alloy was machined with central composite design-based experimental methodology. Ultrasonic power was varied in steps from 20 to 100% at different speeds, depth of cuts and feed rates. It was concluded that axial cutting force is affected by ultrasonic power. Halim et al. (2017) finished CFRP composites with and without the application of ultrasonic energy in milling. Tool wear, surface roughness, cutting forces and machining temperatures were studied at constant machining (speed, feed and depth of cut) and ultrasonic parameters (frequency and amplitude). The outcomes of the research revealed reduction in cutting forces, temperature but an increase in surface roughness and tool wear. The increment in surface roughness is attributed to the application of vibrations perpendicular to feed direction rather than along the feed direction.

A thorough review was authored by Brehl and Dow (2008) on ultrasonic vibration assisted turning (UVAT). In this study, UVAT is extensively reviewed with the available as well as ongoing research. The advantage of using ultrasonic assistance to turning is emphasized in this study. The effect of machining and vibration parameters in turning of Inconel 718 was investigated by Nath and Rahman (2008). The tool work contact ratio (TWCR) is identified to play a significant role on machining performance. Effect of amplitude, frequency and cutting speed on TWCR was studied. It was recognized that amplitude and frequency are inversely proportional and cutting speed is directly proportional to the TWCR. Cutting forces, tool wear and surface roughness were reduced in ultrasonic turning compared to conventional turning. This is attributed to the reduction in TWCR. The combined effect of machining parameters, vibration parameters, tool type and cooling method on the ultrasonic assisted turning was studied by Sui et al. (2021). In this work, a through theoretical and experimental analysis was done. It was suggested that the moderate rotational speed, lower feeds and depth of cut, higher amplitude and HPC cooling yield better performance of the ultrasonic cutting process.

Development of ultrasonic drilling module was done by Moghaddas et al. (2018). Thrust force, torque, surface roughness and quality of hole were studied at constant cutting speed and full amplitude (100%). It was identified that as the amplitude increases, the thrust force reduced by 42% and torque was reduced by 24% and surface finish was improved by 53%. Accuracy of hole was not affected by application of ultrasonics. The application of ultrasonic vibrations to micro milling led to the reduction in the surface roughness in comparison with micro milling without vibrations in the work carried out by Lian et al. (2013). In this work, longitudinal vibrations were applied to the work piece. It was identified that amplitude plays a major role in enhancing the process performance. Llanos et al. (2018) conducted studies on cutting forces in ultrasonic machining of Ti6Al4V. The application of ultrasonic assistance to conventional turning yielded better results by reducing cutting forces. Ultrasonic parameters and the cutting parameters were varied and their effect on cutting force was identified. It was concluded that critical velocity and amplitude are the key contributors for force reduction. Nestler and Schubert (2014) investigated the directional effect of ultrasonic vibrations in turning aluminium metal matrix composites. The surface roughness and residual stresses were studied at constant feed and depth of cut with varying cutting speeds and amplitudes in all the three directions. It was recognized that application of vibrations in the circumferential direction yielded better results than axial direction. It was also reported that higher amplitude led to compressive residual stress.

The frequency also plays a vital role in the ultrasonic machining process along with amplitude. The influence of frequency and spindle speed on thrust force, cutting temperature and quality of hole were investigated by Wei and Wang (2019). In the study, the performance of ultrasonic assisted drilling (UAD) is compared with the conventional drilling process on Ti–6Al–4V/Al2024–T351 laminated material. It was identified that thrust force and cutting temperatures were reduced in both materials with increase in frequency. Similarly the quality of hole also improved. Simulation and experimental studies were conducted by Wang and Wang (2020) with 90°, 120°, 140° point angle, keeping helix angle and drill diameter constant. Rotational speed, feed rate and frequency were varied. Irrespective of feed rate and point angles, the thrust force and temperature in UAD is less compared to conventional drilling. The increment of frequency resulted in decrease of thrust force and temperature. In addition the cutting temperature was reduced by a maximum of 31.10% which is attributed to the intermittent movement of the drill by application of vibrations. Effective stress is also reduced in UAD. Ultrasonic milling was studied on SiCp/Al composites by Xiang et al. (2019) using finite element analysis. The effect of frequency and amplitude were investigated as a part of the study. The necessity of using appropriate

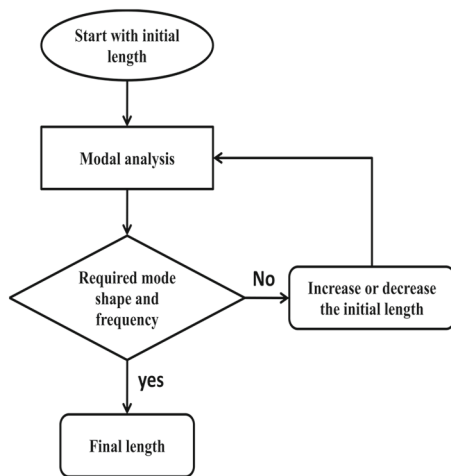


**Fig. 2** Schematic representation of modal analysis for determining the horn length

amplitude is emphasized. Using higher frequency, reduced the crack growth and smoothed the particle breakage. Ultrasonic milling generated lesser temperatures than its counterpart. It was also reported that increase in amplitude led to a reduced temperature.

In the context of horn design, modal and harmonic analysis are essential in designing the horn to achieve maximum efficacy (Kaul et al. 2018). As the complexity of horn shape increases the analytical method will be tedious and time consuming. This is addressed by the finite element method which is widely found and accepted in the literature. Using any commercial finite element packages like ANSYS, COMSOL, NASTRAN, etc., the modal analysis of complex horns is made easy. The schematic shown in the Fig. 2 illustrates the process by which length is decided according to modal analysis using finite element method. Roy and Jagadish (2017) designed hollow circular exponential horn to resonating length using modal analysis. In the work carried out by Zhao et al. (2021), finite element analysis was adopted to investigate the mode of vibration and resonating frequency of the ultrasonic horn. The optimum sized horn designed in the study, also resulted in minimum induced stresses. Singh et al. (2019) analyzed stepped and conical horn profiles for the mode shapes. In this work, aluminium and titanium horns were investigated. It was concluded that titanium horn with stepped profile and aluminium horn with exponential profile have higher natural frequencies. Stănaşel et al. (2014) determined the mode shapes of an ultrasonic welding horn using finite element method. Three mode shapes were determined in this work and the mode close to applied frequency was chosen. It was emphasized that the modal frequencies can be determined with tolerance of 500 Hz. The choice of choosing an appropriate mode from the available mode shapes was emphasized by Satpathy et al. (2016). A stainless steel horn

with eight different profiles was studied by Kumar Patel et al. (2020) using finite element analysis. In this study, magnification factor and developed stresses were taken as performance measures. Modal and harmonic analysis were carried out on all the horn profiles. Horn profile with cylindrical and exponential combination was proved to be better design. Jagadish and Ray (2018) performed harmonic analysis in determining the amplification factor and induced stresses. A longitudinally varying rectangular horn is designed and analyzed for ultrasonic machining. In addition to mode shapes and dynamic characteristics, the choice of horn material for maximizing magnification factor was also determined using finite element analysis by Chandan and Sahoo (2021). Of the five materials tested, aluminium showed higher magnification followed by titanium. The low damping coefficient of aluminium is attributed for its better performance. A novel approach of integrating finite element and artificial neural network methods was used in the design of ultrasonic horn by Shahid et al. (2020). In this work, the role of groove variables on the performance of longitudinal-torsional mode horn was studied. It was concluded that depth of the groove is most influencing parameter on resonating frequency and torsionality. The optimum groove variables are then decided for yielding maximum torsionality using artificial neural network. Along with the aforementioned analysis, mechanical impedance (Stănaşel et al. 2014), acoustic impedance tests (Shakeeb and Sarraf 2019) were also available in the literature. These tests ensure proper contact of sonotrode (booster plus horn) with the transducer and within the sonotrode itself. Fatigue tests and thermo elastic tests were also (Roopa Rani et al. 2015) performed to ensure the proper working of horn under fatigue loads (welding, etc.) and to withstand internal heat generation.

The literature study reveals the importance of amplitude and frequency in ultrasonic machining. This emphasizes the role of horn design in successful implementation of ultrasonic vibrations to enhance a machining process. A proper horn design will ensure lower TWCR and hence improves the machining process. However, most of the literature covers design and analysis of simple horn profiles like circular, stepped, exponential, etc. Design and analysis of higher order and complex horn profiles are least discussed. Also the roles of geometrical parameters of the horn like diameter, length proportions were not investigated in complex profiles. In this work, an attempt is made to design horn with higher order profiles with variation in its diameter and length proportions. The paper also aims to design, analyze and identify an efficient horn with higher amplification factor and lower stress. Single exponential and double exponential horns (referred as SEH and DEH hereafter) with different tool end diameters and length proportions were designed and analyzed. The study is focused on the effect of diameter ratio of horn, horn profile (SEH, DEH) and length variation within the horn

**Table 1** List of materials used in manufacturing of horn

S. No	Material	Young's modulus ' $E$ '	Density ' $\rho$ '	Acoustic speed ' $C$ '
–	–	GPa	kg/m <sup>3</sup>	mm/s
1	Titanium alloys (Ti6Al4V) (Singh et al. 2019) (Chu et al. 2018)	115	4420	5,100,794
2	C45 steel (Stănăşel et al. 2014)	210	7800	5,188,745
3	Stainless steel (Chhabra et al. 2016)	180	8000	4,743,416
4	Aluminium (Singh et al. 2019)	71	2710	5,118,521
5	Monel (Roopa Rani et al. 2015)	192	8800	4,670,994
6	Mild steel (Vivekananda et al. 2014)	210	7861	5,188,745

(DEH2575, DEH5050 and DEH7525) on the total deformation, amplification factor and effective stress. The mixed horn profiles (cylindrical plus exponential) are then analyzed. Harmonic analysis revealed the characteristics of the proposed horn designs. The finite element method was adopted in analyzing all the horn designs with assumptions that the material is homogenous, isotropic, defect free. The acoustic losses if any, at the joining of transducer-booster and booster-horn are negligible.

## 2 Design of horn

The design of horn in an ultrasonic machining setup plays a major role in enhancing the machining performance in terms of increased tool life, cutting force reduction, improved surface texture, and reduced cutting temperatures by magnification of amplitude. The horn not only amplifies the amplitude, but also concentrates the ultrasonic energy at desired location (cutting tool). The governing differential equation in the horn design is given in Eq. (1) where ' $a$ ' is the amplitude,  $A(x)$  is the area of cross section, ' $\omega$ ' is the angular velocity and ' $C$ ' is the acoustic speed.

$$\frac{d^2 a}{dx^2} + \frac{d \ln A(x)}{dx} \frac{da}{dx} + \frac{\omega^2}{C^2} a = 0. \quad (1)$$

The dominant factors in the design of an ultrasonic horn are frequency, and amplification factor. These are mainly influenced by horn material, horn length, horn profile, diameters at fixed end (booster end) and tool end. These are discussed in detail in this section.

### 2.1 Horn material

The choice of horn material depends on the ability of it to allow the acoustic waves through it, i.e., acoustic speed. This

depends on Young's modulus and density of the material. The relation between acoustic speed and aforementioned parameters is given by Eq. 2. The materials used for horn manufacturing mentioned in the literature are quoted in Table 1. The horn materials are chosen based on high fatigue strength and low acoustic losses (Roy and Jagadish 2017; Stănăşel et al. 2014). The weight of the horn is also considered in choosing material. In spite of the good acoustic properties, the stainless steel horns are having higher weight compared to titanium horns (Roopa Rani et al. 2015).

$$C = \sqrt{\frac{E}{\rho}}. \quad (2)$$

### 2.2 Horn length

The horn length is independent of magnification factor but it affects the frequency. The length is calculated either by mathematical expression or through finite element method. The horn length should allow resonance at the applied frequency (Roy and Jagadish 2017). For stepped, cylindrical and exponential horns, the resonating length is calculated using the equations in Table 2. For complex shapes where analytical calculation is cumbersome, it is initially calculated using the expressions in Table 2 or using past experience and then adjusted to resonating length (Satpathy et al. 2016).

### 2.3 Horn profile

Horns of different shapes are seldom available in the literature. Although some researchers evaluated different horn shapes for various applications, the magnification factor is the governing parameter in finalizing the dimensions as well as horn profile (He et al., 2015). Some basic profiles available in the literature are summarized below in Table 3.

**Table 2** Expressions for calculating horn length

S. No	Shape	Expression for horn length (l)
1	Cylindrical stepped horn (Vivekananda et al. 2014)	$l = \frac{c}{2f}$
2	Circular exponential horn (Youssef and El-Hofy 2008)	$l = \frac{c}{2f} \sqrt{1 + \left(\frac{\ln\left(\frac{D_o}{D_i}\right)}{\pi}\right)^2}$

**Table 3** Different types of Horn profiles

S. No	Horn profile	Geometric parameters	Applied frequency (kHz)
1.	Stepped (Vivekananda et al. 2014)	$D = 40$ mm $d = 20$ mm $l = 129$ mm	$20 \pm 0.5$ kHz
2.	Exponential, hollow exponential (Roy and Jagadish 2017)	$D = 40$ mm $d = 10$ mm $d_h = 5$ mm (hole dia) $l = 120.69$ mm	23.5 kHz
3.	B spline (Nguyen et al. 2014)	$R_1/R_2 = 4$ $l = 95$ mm	28.0 kHz
4.	Rectangular profile (Jagadish and Ray 2018)	$W_1/W_2 = 4$ $l_1/l_2 = 0.2$ $l = 118.61$ mm	23.5 kHz
5.	Higher order horn profile (Chhabra et al. 2016)	$D = 50$ mm $d = 12.5$ mm $l = 125$ mm	20 kHz
6.	Biezer curve (Wang and Nguyen 2014)	$W_1 = 20$ mm $W_2 = 1.5$ mm $t = 1.2$ mm $l = 94$ mm	28.0 kHz
7.	Conical (He et al. 2015)	$D/r = 6.36$ $l = 53$ mm	53.7 kHz

**2.4 Amplification factor**

The performance of the horn is evaluated through amplification factor also called as gain (Tadvi et al. 2015). It is the ratio of output amplitude (tool end) to the input amplitude(booster end) as expressed in Eq. 3 (Roy and Jagadish 2017; Jagadish and Ray 2018). The amplification factor can be calculated from the horn dimensions for simple horn shapes as shown in the Table 4. However for higher order horns with complex geometry, determination of amplification factor becomes more complicated.

$$M = \frac{\text{Output amplitude}}{\text{Input amplitude}} \tag{3}$$

**Table 4** Amplification factor for simple horn shapes

S.No	Shape	Amplification factor ‘m’
1	Cylindrical stepped (Youssef and El-Hofy 2008)	$M\alpha \left(\frac{\text{diameter at larger end}}{\text{diameter at small end}}\right)^2$
2	Circular single exponential	$M\alpha \frac{\text{diameter at larger end}}{\text{diameter at small end}}$
3	Non-Circular single exponential	$M\alpha \sqrt{\frac{\text{Area at larger end}}{\text{Area at small end}}}$

**3 Finite element modeling of the horn**

The ease of calculation, accuracy in results and availability of advanced processing software made the application of finite element simulation more versatile tool in solving many engineering problems. The steps in finite element simulation are preprocessing (geometry, material assignment, discretization), processing (applying boundary conditions and solving) and post processing (evaluation of results). The geometry is modeled in a CAD package and the material is assigned as per the requirement. The type and number of elements is chosen based on the physics of the problem, accuracy of solution needed and computational availability without affecting the solution. The appropriate boundary conditions are imposed on the model to replicate the real-time conditions. The model is then solved and results are evaluated.

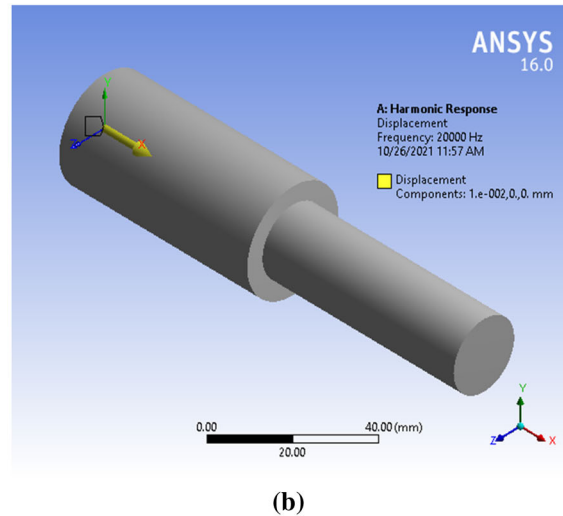
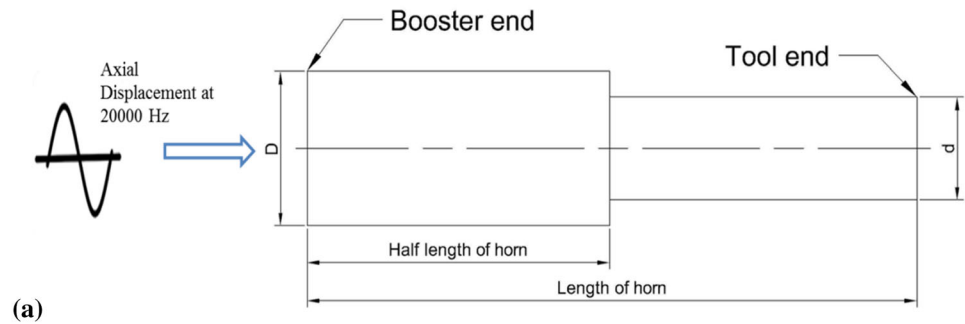
**3.1 Modal analysis**

Modal analysis reveals the modes in which the horn vibrates. The natural frequencies and their respective vibration patterns (mode shapes) of the horn are identified. The horn should be of resonating length to achieve maximum amplification. The operating frequency of the horn is fixed by the generator capacity and horn should be of resonating length at that frequency. Hence the natural frequency of the horn and excitation frequency must match. In this analysis, the horn length is calculated based on the excitation frequency and hence assumed to vibrate at the same. Therefore further adjustment in length through modal analysis is not focused.

**3.2 Harmonic analysis**

The horn with the finalized length is tested for induced stresses and deformation with required boundary conditions through harmonic analysis as represented in Fig. 3a, b. Using the displacement constraint, a known displacement of 10 μm was applied along the axial direction at the booster end and displacements in other directions are kept zero. The frequency of 20,000 Hz is applied in sinusoidal form using the analysis settings and the developed stresses, deformation and

**Fig. 3** **a** Schematic representation of boundary conditions used in the analysis. **b** Application of boundary conditions in the analysis



amplitude are evaluated. The dynamic behavior of the horn is thus studied.

A total of 28 designs were simulated and analyzed including the horn supplied by the manufacturer, i.e., 30–20-sepped horn. The governing equations for the horn profiles are provided in the Table 5. All the designs were modeled and analyzed in ANSYS 16 as shown in Fig. 4. The element chosen was Solid 187. Harmonic analysis was done on all the horn designs and the best profile was identified on the higher amplification and lower stress criteria. Titanium alloy is chosen as horn material for simulation. The properties of the titanium alloy are mentioned in the Table 1. The use of titanium alloy as horn material is well justified in the literature (Roy and Jagadish 2017) because of its higher fatigue strength and low acoustic losses. The dimensions of the horn are based on the physical constraints. The larger diameter ( $D$ ) is fixed by the booster diameter as 30 mm. The lower diameter ( $d$ ) is varied from 10 mm up to 20 mm in steps of 2.5 mm. The diameter is not reduced below 10 mm, as tool is to be fitted at this location. The designs were carried out by fixing the major diameter of the horn (booster end) and the lower end (tool end) diameter is varied. The length for single exponential horn is calculated based on the standard expression given in the Table 2. The double exponential horns are assumed with this same length. The boundary conditions are

then applied depending on physical conditions of the horn. Amplitude of  $10 \mu\text{m}$  is applied at the booster end in the axial direction. All the DOF except axial movement are fixed at the booster end and lower end of the horn is unconstrained. This ensures the horn is vibrated axially and the vibration in the other directions is negligible.

### 3.3 Validation of the model

The developed model is then validated with the experimental value of amplitude measured at the tool end of the horn of ultrasonic vibration assisted machining set up available in the laboratory. The horn is made of Titanium alloy. The measurements are taken using an accelerometer connected to an Indi6192 digital vibration meter. The measured value of amplitude from this experimental set up is  $25 \mu\text{m}$  and it is in line with the supplier calibration data (amplitude of  $25 \mu\text{m}$  at the tool end at 20,000 Hz). The horn is modeled with the dimensions from the manufacturer (30–20-stepped horn) and subjected to similar boundary conditions, i.e., axial displacement of  $10 \mu\text{m}$  at 20000 Hz at the boosted end in the simulation. The amplitude at the tool end is measured and found to be  $23.05 \mu\text{m}$ . On comparison, the simulated model reported an error of 7.8% which is within the acceptable limit. Furthermore, the simulation results revealed that

**Table 5** Governing equations for horn profiles

Diameter ratio	Profile	Length	Governing equation	
30–10	Single Exponential Horn	134.48	$D(x) = D_0e^{-hx}$ $0 \leq x \leq 134.48$ $h = 0.0081$	
	Double Exponential horn 2575	134.48	$y = e^x$ $y = e^{\frac{x-3.5151}{1.4025}} + e^{3.5151} - 1$ $0 \leq x \leq 3.5151$ $3.5151 \leq x \leq 5$	
	Double Exponential horn 5050	134.48	$y = e^x$ $y = e^{\frac{x-4.2082}{1.3714}} + e^{4.2082} - 1$ $0 \leq x \leq 4.2082$ $4.2082 \leq x \leq 5$	
	Double Exponential horn 7525	134.48	$y = e^x$ $y = e^{\frac{x-4.6137}{1.5196}} + e^{4.6137} - 1$ $0 \leq x \leq 4.6137$ $4.6137 \leq x \leq 5$	
	Cylindrical-exponential horn 2575	128	$D = D_0$ $D(x) = D_0e^{-hx}$ $0 \leq x \leq 32$ $32 \leq x \leq 128$ $h = 0.0114$	
	Cylindrical-exponential horn 5050	128	$D = D_0$ $D(x) = D_0e^{-hx}$ $0 \leq x \leq 64$ $64 \leq x \leq 128$ $h = 0.0171$	
	Cylindrical-exponential horn 7525	128	$D = D_0$ $D(x) = D_0e^{-hx}$ $0 \leq x \leq 96$ $96 \leq x \leq 128$ $h = 0.0343$	
	Stepped	125	$D = D_0$ $D = D_i$ $0 \leq x \leq 62$ $63 \leq x \leq 125$	
	30–12.5	Single Exponential Horn	132.36	$D(x) = D_0e^{-hx}$ $0 \leq x \leq 8.75$ $h = 0.0066$
		Double Exponential horn 2575	132.36	$y = e^x$ $y = e^{\frac{x-3.499}{1.1395}} + e^{3.499} - 1$ $0 \leq x \leq 3.499$ $3.499 \leq x \leq 8.75$
Double Exponential horn 5050		132.36	$y = e^x$ $y = e^{\frac{x-4.192}{1.0832}} + e^{4.192} - 1$ $0 \leq x \leq 4.192$ $4.192 \leq x \leq 8.75$	
Double Exponential horn 7525		132.36	$y = e^x$ $y = e^{\frac{x-4.597}{1.176}} + e^{4.597} - 1$ $0 \leq x \leq 4.597$ $4.597 \leq x \leq 8.75$	
30–15	Single Exponential Horn	130.58	$D(x) = D_0e^{-hx}$ $0 \leq x \leq 7.5$ $h = 0.0053$	
	Double Exponential horn 2575	130.58	$y = e^x$ $y = e^{\frac{x-3.4856}{0.8737}} + e^{3.4856} - 1$ $0 \leq x \leq 3.4856$ $3.4856 \leq x \leq 7.5$	
	Double Exponential horn 5050	130.58	$y = e^x$ $y = e^{\frac{x-4.1788}{0.7918}} + e^{4.1788} - 1$ $0 \leq x \leq 4.1788$ $4.1788 \leq x \leq 7.5$	
	Double Exponential horn 7525	130.58	$y = e^x$ $y = e^{\frac{x-4.5843}{0.8292}} + e^{4.5843} - 1$ $0 \leq x \leq 4.5843$ $4.5843 \leq x \leq 7.5$	
30–17.5	Single Exponential Horn	129.38	$D(x) = D_0e^{-hx}$ $0 \leq x \leq 6.75$ $h = 0.0041$	
	Double Exponential horn 2575	129.38	$y = e^x$ $y = e^{\frac{x-3.4701}{0.3341}} + e^{3.4701} - 1$ $0 \leq x \leq 3.4701$ $3.4701 \leq x \leq 6.75$	
	Double Exponential horn 5050	129.38	$y = e^x$ $y = e^{\frac{x-4.1696}{0.4791}} + e^{4.1696} - 1$ $0 \leq x \leq 4.1696$ $4.1696 \leq x \leq 6.75$	
	Double Exponential horn 7525	129.38	$y = e^x$ $y = e^{\frac{x-4.575}{0.4776}} + e^{4.575} - 1$ $0 \leq x \leq 4.575$ $4.575 \leq x \leq 6.75$	

Table 5 continued

Diameter ratio	Profile	Length	Governing equation		
30–20	Single Exponential Horn	128.57	$D(x) = D_0 e^{-hx}$	$0 \leq x \leq 128.57$ $h = 0.0031$	
	Double Exponential horn 2575	128.57	$y = e^x$ $y = e^{\frac{x-3.4701}{0.3341}} + e^{3.4701} - 1$	$0 \leq x \leq 3.4701$ $3.4701 \leq x \leq 5$	
	Double Exponential horn 5050	128.57	$y = e^x$ $y = e^{\frac{x-4.1632}{0.2002}} + e^{4.1632} - 1$	$0 \leq x \leq 4.1632$ $4.1632 \leq x \leq 5$	
	Double Exponential horn 7525	128.57	$y = e^x$ $y = e^{\frac{x-4.5687}{0.12317}} + e^{4.5687} - 1$	$0 \leq x \leq 4.5687$ $4.5687 \leq x \leq 5$	
	Cylindrical-exponential horn 2575	126.96	$D = D_0$ $D(x) = D_0 e^{-hx}$	$0 \leq x \leq 31.74$ $31.74 \leq x \leq 126.96$ $h = 0.0042$	
		Cylindrical-exponential horn 5050	126.96	$D = D_0$ $D(x) = D_0 e^{-hx}$	$0 \leq x \leq 63.48$ $63.48 \leq x \leq 126.96$ $h = 0.0063$
			Cylindrical-exponential horn 7525	126.96	$D = D_0$ $D(x) = D_0 e^{-hx}$
	Stepped (Horn supplied by manufacturer)	125	$D = D_0$	$0 \leq x \leq 62$	
			$D = D_i$	$62 \leq x \leq 125$	

the horn supplied by the manufacturer is having a maximum stress of 124.31 MPa. The validation results are depicted in Fig. 5.

## 4 Results and discussion

The horns are allowed to vibrate in axial mode at 20000 Hz with one end fixed and other end free. The total deformation, effective stress and amplification of the horns obtained from simulation are presented in this section. The effect of diameter ratio, horn profile and length variations (in case of DEH) on the aforementioned parameters are discussed. The simulation results are summarized in the Table 6.

### 4.1 Effect of diameter ratio

The effect of diameter ratio on the total deformation and effective stress along the horn length are discussed in this section. SEH and DEH-5050 were considered in the analysis. The deformation and effective stress plots are presented in Tables 7 and 8 respectively.

The deformation along the length for SEH with different diameter ratio is shown in Fig. 6. The trend in the deformation along the length of the horns is similar in all cases but more deformation is observed in horns with lower tool end diameters. This gives more amplification for lower tool end diameter horns which is evident from the Fig. 7. As the tool end diameter reduces, the strength of the horn decreases that

offers lower resistance to applied vibration. Thus the deformation is increased. The variation in effective stress in SEH for all diameters along the length is plotted in Fig. 8. Variation of stress along the length is not only similar for all the horns but also smooth variation can be observed. However the stress magnitude is increasing with reduced tool end diameter from 20 to 10 mm. Also an average increment of 8.6% in stress is identified within SEH horns with variation in diameter from 20 to 10 mm. As the resisting area is reduced with reduction in tool end diameter of the horns, and the applied energy being constant throughout the horn length, the stress is increased. It is noteworthy that their magnitude in all the cases is well below endurance limit of horn material which is 382 MPa (Roy and Jagadish 2017).

In DEH, the effect of diameter ratio on deformation is presented in the Fig. 9. The deformation plot suggests a similar behavior with SEH indicating an inverse relation between tool end diameter and deformation. But the magnitude of deformation is more in DEH than SEH leading to more amplification in the former as evident from the Fig. 10. Also the increment in deformation between each diameter is also more in case of DEH. The effective stress plot along the horn length as depicted in Fig. 11 indicates a clear rise in the stress halfway from the booster end. Though a similar pattern is observed, the variation is smoother with higher tool end diameter horns (20 mm). Peak stresses can be observed with increasing magnitude as the tool end diameter gets reduced. The change in cross section at the middle of the horns resulted in stress concentration causing a sudden jump



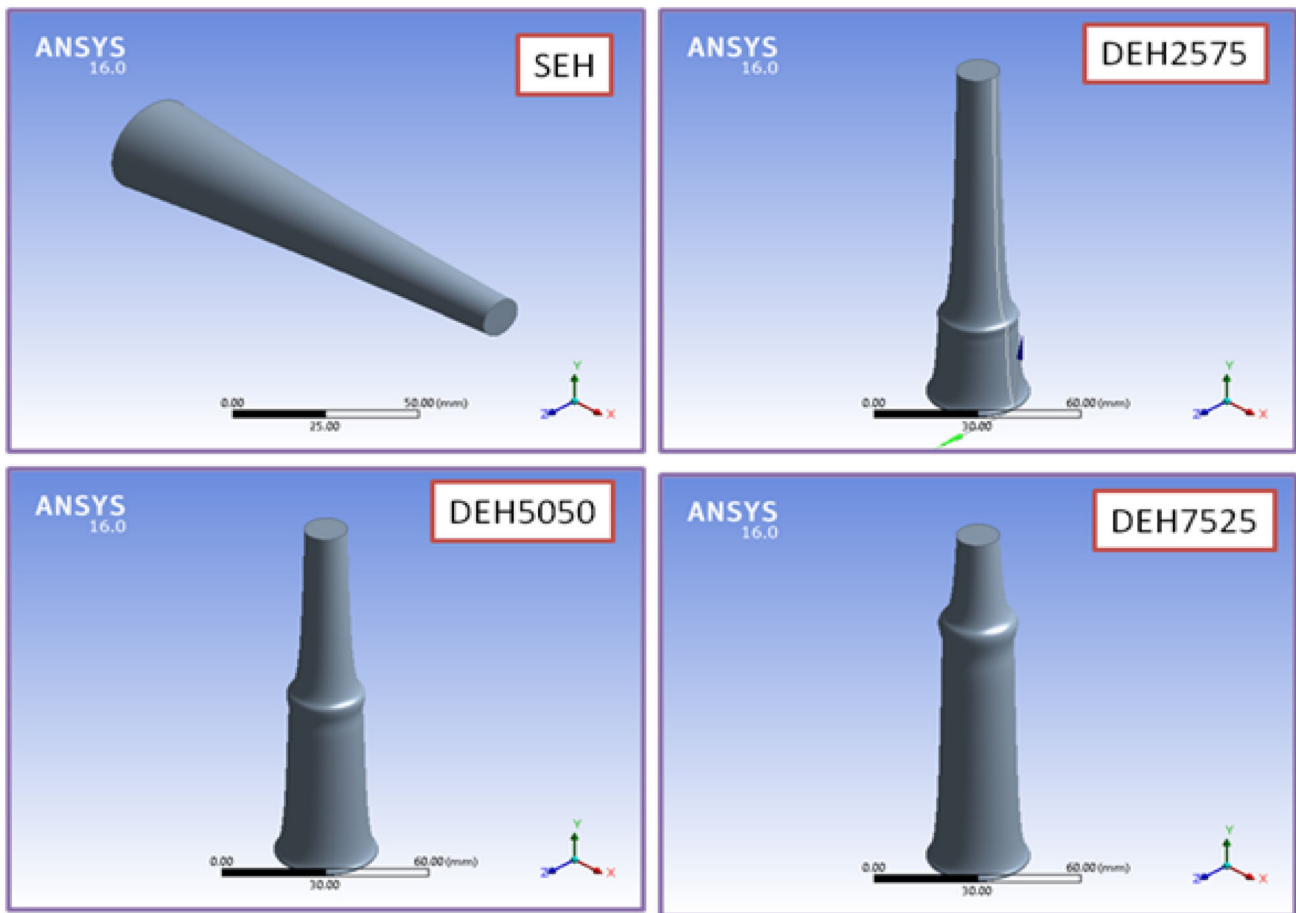


Fig. 4 Different profiles of Horn (SEH and DEH)

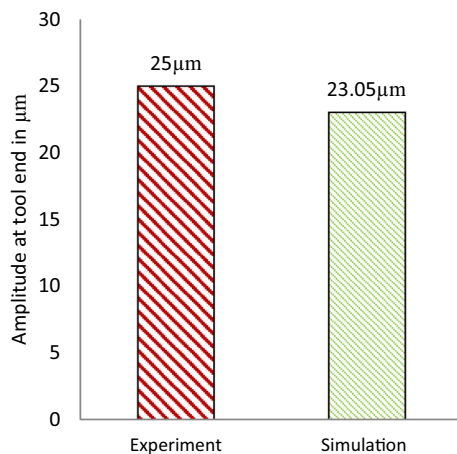


Fig. 5 Comparison of the simulated model with experimental value

in the stresses at the same location. An average of 15.66% of stress is reduced within DEH when the tool end diameter is varied from 10 to 20 mm. Though the stresses are high in DEH, they are well below the endurance limit of the horn material like in the case of SEH.

#### 4.2 Effect of variation in profile

The profile variation is plotted at constant tool end diameter of 10 mm as the amplification, effective stress, deformation are more at lower tool end diameters. The profiles considered are SEH, DEH-5050, Step and Cyl + Exp-5050. The variation in length is kept constant by choosing 5050 variation. The deformation and effective stress plots are shown in Table 9. The total deformation along the length for aforementioned profiles was depicted in the Fig. 12. The deformation is more in stepped profile and well beyond the other profiles. This is in agreement with the literature (Amin and Youssef 1995). The higher deformation in stepped profile is due the reduced diameter up to half length that reduced its strength causing more deformation. From the Fig. 13, amplification is more in stepped profile with 11.93 followed by 3.599 for DEH-5050 as it is also a function of deformation. The effective stress is also very high in stepped profile with 323.21 MPa followed by DEH-5050 with 68.42 MPa as shown in Fig. 14. The variation in stress in other profiles is comparatively less. The steep increase in stress after half of its length from the booster end in stepped horn is due to the low resisting area

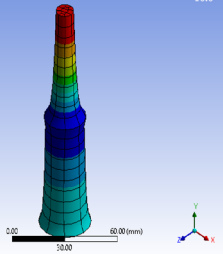
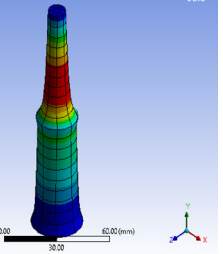
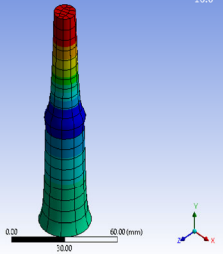
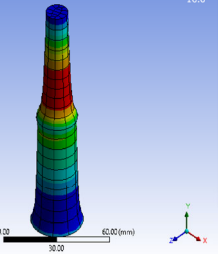
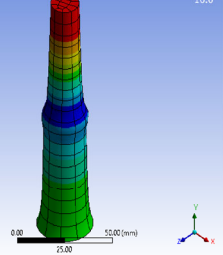
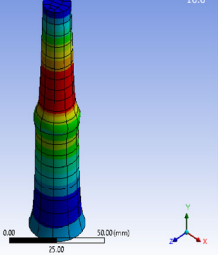
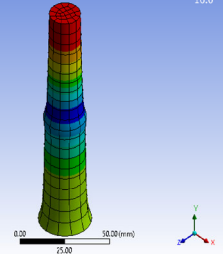
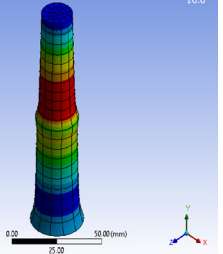
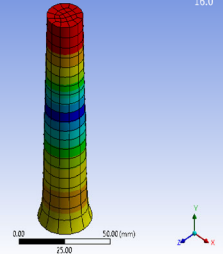
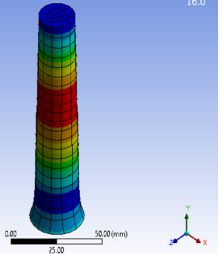
**Table 6** Detailed summary of various horn profiles simulated

S. No	Diameter ratio	Horn profile	Total deformation $\mu\text{m}$	Effective stress MPa	Amplification factor –
1	30–10	Single Exponential Horn	28.29	50.71	2.82
		Double Exponential Horn 2575	26.24	57.29	2.62
		Double Exponential Horn 5050	35.99	68.42	3.59
		Double Exponential Horn 7525	15.68	30.80	1.56
		Cylindrical—exponential 2575	35.76	58.05	3.57
		Cylindrical—exponential 5050	21.85	30.35	2.18
		Cylindrical—exponential 7525	12.21	27.53	1.22
		Stepped	119.30	323.21	11.93
2	30–12.5	Single Exponential Horn	23.33	44.65	2.33
		Double Exponential Horn 2575	21.01	48.22	2.10
		Double Exponential Horn 5050	27.50	56.69	2.75
		Double Exponential Horn 7525	15.24	30.83	1.52
3	30–15	Single Exponential Horn	19.85	40.43	1.98
		Double Exponential Horn 2575	17.56	42.20	1.75
		Double Exponential Horn 5050	21.41	47.55	2.14
		Double Exponential Horn 7525	13.80	32.73	1.38
4	30–17.5	Single Exponential Horn	17.32	37.30	1.73
		Double Exponential Horn 2575	14.84	37.03	1.48
		Double Exponential Horn 5050	16.88	39.86	1.68
		Double Exponential Horn 7525	13.84	31.36	1.38
5	30–20	Single Exponential Horn	15.34	34.70	1.53
		Double Exponential Horn 2575	12.54	32.31	1.25
		Double Exponential Horn 5050	13.43	33.89	1.34
		Double Exponential Horn 7525	12.77	31.44	1.27
		Cylindrical—exponential 2575	16.78	36.01	1.67
		Cylindrical—exponential 5050	14.81	29.66	1.48
		Cylindrical—exponential 7525	11.60	27.52	1.16
		Stepped (Horn supplied by manufacturer)	23.05	124.31	2.30

**Table 7** Total deformation and effective stress plots for SEH with different diameter ratio

Profile	Total Deformation	Effective stress
30-10-SEH		
30-12.5-SEH		
30-15-SEH		
30-17.5-SEH		
30-20-SEH		

**Table 8** Total deformation and effective stress plots for DEH with different diameter ratio and same length variation

Profile	Total Deformation	Effective stress
30-10-DEH5050	<p>ANSYS 16.0</p> <p>C-Harmonic Response Total Deformation Type: Total Deformation Frequency: 20000 Hz Sweeping Phase: 0 ° Unit: mm 5/6/2020 7:59 PM</p> <p>0.039991 Max 0.010862 0.028933 0.024295 0.020276 0.016347 0.012418 0.008489 0.004561 0.00063251 Min</p> 	<p>ANSYS 16.0</p> <p>C-Harmonic Response Equivalent Stress Type: Equivalent (von-Mises) Stress Frequency: 20000 Hz Sweeping Phase: 0 ° Unit: MPa 5/6/2020 7:50 PM</p> <p>66.429 Max 62.095 53.34 43.66 35.02 30.437 22.883 15.288 7.674 0.019552 Min</p> 
30-12.5-DEH5050	<p>ANSYS 16.0</p> <p>A-Harmonic Response Total Deformation Type: Total Deformation Frequency: 20000 Hz Sweeping Phase: 0 ° Unit: mm 6/4/2020 9:54 PM</p> <p>0.027391 Max 0.024596 0.021534 0.0182 0.015226 0.012332 0.009531 0.006542 0.003554 0.0005647 Min</p> 	<p>ANSYS 16.0</p> <p>A-Harmonic Response Equivalent Stress Type: Equivalent (von-Mises) Stress Frequency: 20000 Hz Sweeping Phase: 0 ° Unit: MPa 6/4/2020 9:54 PM</p> <p>56.099 Max 50.423 44.106 37.91 31.513 25.317 18.981 12.684 6.3279 0.019319 Min</p> 
30-15-DEH5050	<p>ANSYS 16.0</p> <p>A-Harmonic Response Total Deformation -10000 Hz Type: Total Deformation Frequency: 20000 Hz Sweeping Phase: 0 ° Unit: mm 6/5/2020 5:55 PM</p> <p>0.024414 Max 0.019885 0.01575 0.011646 0.012897 0.009789 0.007516 0.005104 0.002762 0.00045182 Min</p> 	<p>ANSYS 16.0</p> <p>A-Harmonic Response Equivalent Stress -20000 Hz Type: Equivalent (von-Mises) Stress Frequency: 20000 Hz Sweeping Phase: 0 ° Unit: MPa 6/5/2020 5:55 PM</p> <p>42.559 Max 42.277 36.996 31.715 26.433 21.152 15.87 10.589 5.3075 0.026135 Min</p> 
30-17.5-DEH5050	<p>ANSYS 16.0</p> <p>A-Harmonic Response Total Deformation -10000 Hz Type: Total Deformation Frequency: 20000 Hz Sweeping Phase: 0 ° Unit: mm 6/23/2020 12:56 AM</p> <p>0.019689 Max 0.015867 0.012524 0.011441 0.008677 0.007045 0.0060014 0.0041882 0.002371 0.00056188 Min</p> 	<p>ANSYS 16.0</p> <p>A-Harmonic Response Equivalent Stress -20000 Hz Type: Equivalent (von-Mises) Stress Frequency: 20000 Hz Sweeping Phase: 0 ° Unit: MPa 6/23/2020 12:56 AM</p> <p>39.866 Max 39.438 34.811 29.533 24.155 17.789 13 8.8722 4.4445 0.01679 Min</p> 
30-20-DEH5050	<p>ANSYS 16.0</p> <p>A-Harmonic Response Total Deformation Type: Total Deformation Frequency: 20000 Hz Sweeping Phase: 0 ° Unit: mm 5/6/2020 9:19 PM</p> <p>0.01343 Max 0.011872 0.010314 0.008853 0.007969 0.006186 0.004882 0.003219 0.001655 0.00038519 Min</p> 	<p>ANSYS 16.0</p> <p>A-Harmonic Response Equivalent Stress Type: Equivalent (von-Mises) Stress Frequency: 20000 Hz Sweeping Phase: 0 ° Unit: MPa 5/6/2020 9:20 PM</p> <p>33.897 Max 30.132 26.947 22.622 18.817 14.972 11.327 7.9419 3.7189 0.011962 Min</p> 

**Fig. 6** Variation of deformation along the length in SEH with different diameter ratio

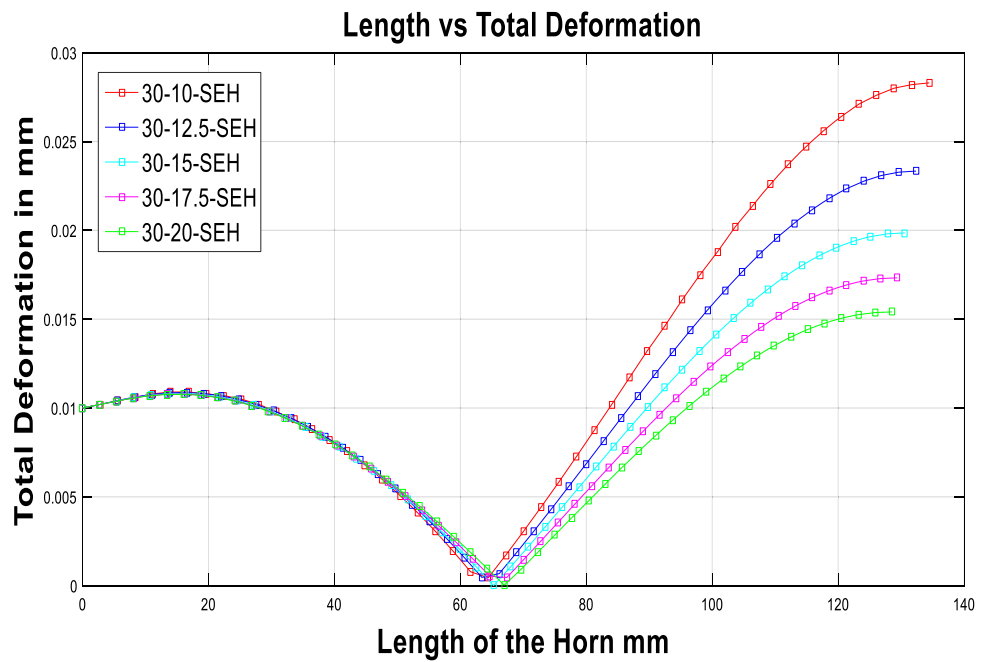
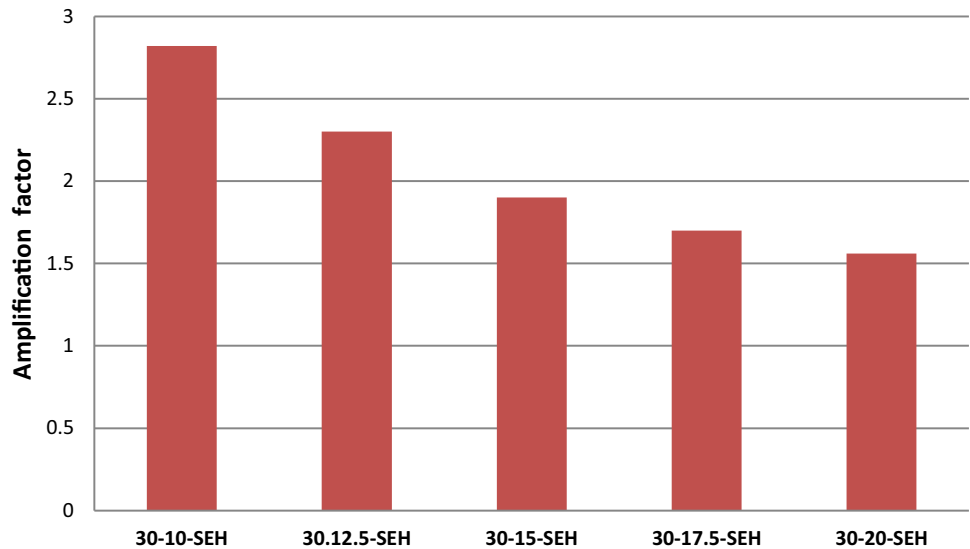


**Fig. 7** Variation of amplification in SEH with different diameter ratio



due to reduced diameter accompanied by an abrupt change in cross section that leads to stress concentration. Apart from stepped profile, the other profiles seemed to be having less impact on the deformation as well as stress.

**4.3 Effect of length variation**

The variation in the length proportion with in a profile is discussed in this section as depicted in Table 10. Horns with DEH profile with tool end diameter of 10 mm are chosen. The effect of length variation in 2575, 5050, 7525 proportions on total deformation, amplification, and effective stress were analyzed. From the deformation plot shown in Fig. 15, 5050 variation is having higher deformation than the others. The

lower deformation in 7525 than its counterparts is because of the higher resisting area occupying greater portion of its length in the former than the later cases. This is applicable for amplification factor also as in Fig. 16. It can be depicted from the stress plot in Fig. 17 that as the profile approaches more uniformity along its length as in 2575 and 7525 variations, smoother variation in stress can be observed.

This is due to less change in the cross section over the length of the horns in the above mentioned cases. In 5050 variation, peak stresses are observed after half length from booster with more non uniformity. The lower stresses in 7525 can be attributed to the more resistance offered than 2575 and 5050 because of larger area of cross section occupying for majority of its length. Thus it can be concluded that the length

**Fig. 8** Variation of effective stress along the length in SEH with different diameter ratio

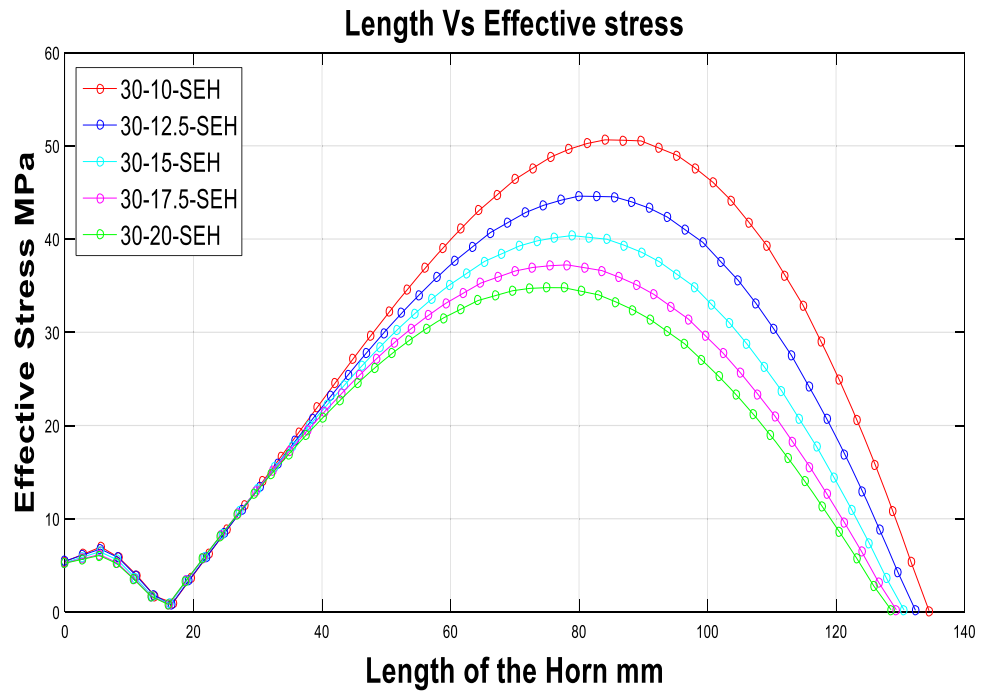
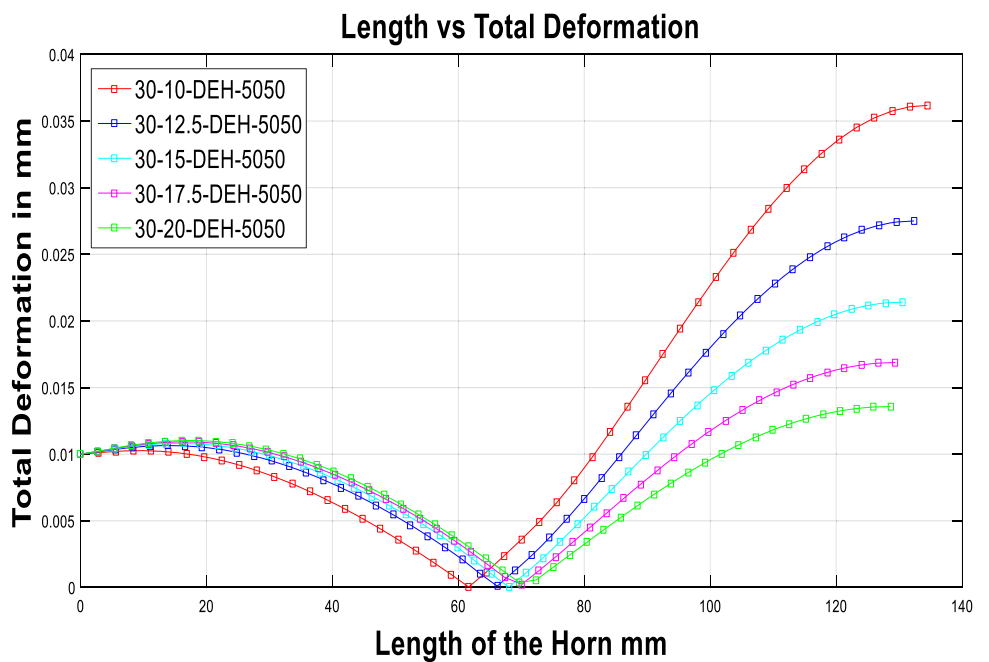


**Fig. 9** Variation of deformation along the length in DEH-5050 with different diameter ratio



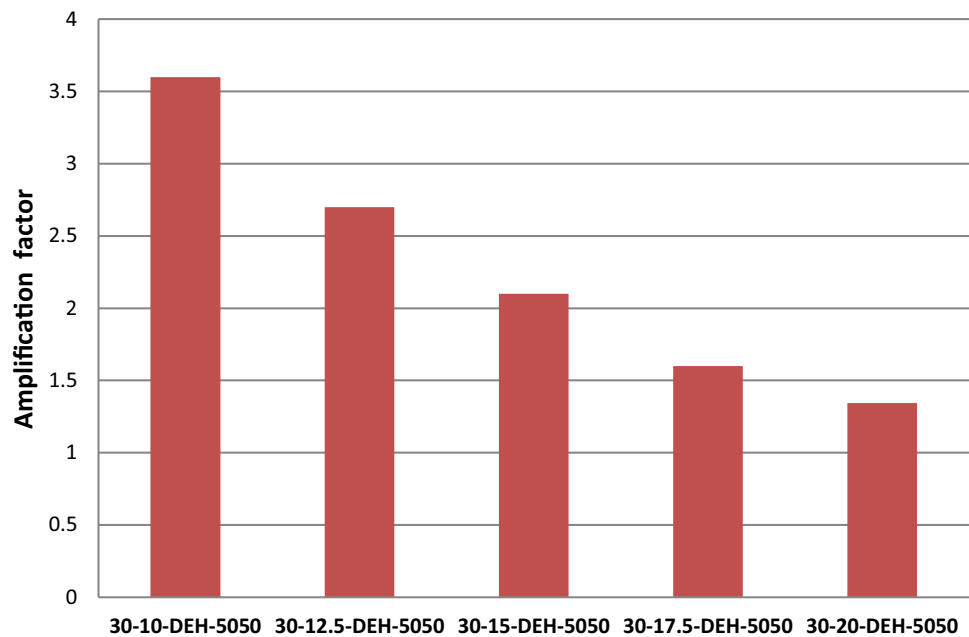
variation that gives more uniformity and greater resisting area will have less deformation as well as stress.

#### 4.4 Mixed horn profiles

Horns with two profiles with dissimilar governing equations are termed as mixed horn profiles. Unlike DEH where two governing equations are exponential in nature, mixed profiles will have two shapes along their length viz., cylindrical

and exponential. In this work, mixed profiles are also studied. The mixed profile consists of cylindrical part to some length and the rest is exponential. Three different proportions namely 2575, 5050, and 7525 are studied with two tool end diameters 10 mm and 20 mm, respectively. The length is calculated based on the standard expression of cylindrical horn and all the cylindrical-exponential horns are assumed of same length. The mixed profiles horns are modeled as shown in the Fig. 18. These are designed with 10 mm and 20 mm tool

**Fig. 10** Variation of amplification in DEH-5050 with different diameter ratio



end diameters. These are analyzed for total deformation and effective stress and plotted in Figs. 19 and 20, respectively. The amplification factor is plotted in Fig. 21. Similar to the earlier profiles lower diameter horns are having more deformation irrespective of profile combinations. The deformation plot also suggests that Cyl + Exp-2575 are performing better than their counterparts for both tool end diameters. The variation in between the profiles of same diameter ratio is more in case of 10-mm tool end diameter horns. This can be seen in amplification also. This also suggests that as the tool end diameter increases, the length variation within the profiles have no significant effect on the performance of mixed horn. Stress plots suggest higher stresses at the lower tool end diameters but the variation along the length is increasing in horns with lower proportion of cylindrical cross section, i.e., 2575 in both cases of 10 mm and 20 mm tool end diameters. But as the cylindrical portion increases as in 5050 and 7525 the stresses are considerably reduced with more uniformity along the length in both 10-mm and 20-mm tool end diameters.

Overall analysis of all the horn designs revealed that the total deformation as well as amplification factor is very high in case of 3010\_stepped horn around 11.93 followed by 30–10–DEH-5050 with 3.59 and 30–10–Cyl + Exp-2575 with 3.57. In spite of the highest amplification, 30–10–Stepped horn is having maximum stress of 323.21 MPa. The stresses in 30–10–Cyl + Exp-2575 is 58.05 MPa which is a little less than 30–10–DEH-5050, i.e., 68.42 MPa. But the stresses in all these horns are well below the endurance limit of horn material, i.e., Ti alloy which is 382 MPa. Hence 30–10–DEH-5050 and 30–10–Cyl + Exp-2575 are chosen as best designs.

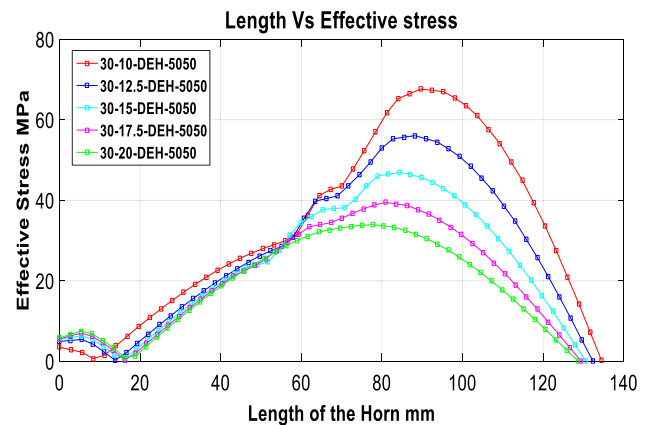


**Fig. 11** Variation of effective stress along the length in DEH-5050 with different diameter ratio

## 5 Conclusions:

The study aimed at modeling and analysis of different horn profiles with different tool end diameters and length variations. Horns with mixed profiles are also included in the study. The influence of diameter ratio, horn profile and length variation within the horn on its performance is studied. Total deformation, effective stress and amplification are considered as performance evaluators in the study. The following are the conclusions drawn from the study:

Horn with tool end diameters from 10 to 20 mm in steps of 2.5 mm are modeled and analyzed. As the tool end diameter is increased, the amplification is reduced and the stresses are more uniform and less in magnitude. SEH and DEH profiles have shown similar trends in terms of diameter variation.

**Table 9** Total deformation and effective stress plots for different profiles with same diameter ratio

Profile	Total Deformation	Effective stress
30-10-SEH	<p>ANSYS 16.0                      A: 3010 Harmonic Response                      Total Deformation                      Type: Total Deformation                      Frequency: 20000 Hz                      Sweeping Phase: 0.°                      Unit: mm                      5/6/2020 8:50 PM                      0.028254 Max                      0.021984                      0.020275                      0.018492                      0.016824                      0.015246                      0.013746                      0.012328                      0.010975                      0.009681                      0.008441                      0.007251                      0.006116                      0.005030                      0.004000</p>	<p>ANSYS 16.0                      A: 3010 Harmonic Response                      Equivalent Stress                      Type: Equivalent (von-Mises) Stress                      Frequency: 20000 Hz                      Sweeping Phase: 0.°                      Unit: MPa                      5/6/2020 8:51 PM                      50.71 Max                      45.084                      39.457                      34.000                      28.600                      23.250                      17.950                      12.700                      7.500                      2.300                      0.000</p>
3010-DEH5050	<p>ANSYS 16.0                      C: Harmonic Response                      Total Deformation                      Type: Total Deformation                      Frequency: 20000 Hz                      Sweeping Phase: 0.°                      Unit: mm                      5/6/2020 7:49 PM                      0.035991 Max                      0.025002                      0.020133                      0.016405                      0.013276                      0.010347                      0.007419                      0.004489                      0.001561                      0.00063251 Min</p>	<p>ANSYS 16.0                      C: Harmonic Response                      Equivalent Stress                      Type: Equivalent (von-Mises) Stress                      Frequency: 20000 Hz                      Sweeping Phase: 0.°                      Unit: MPa                      5/6/2020 7:50 PM                      68.429 Max                      60.035                      53.24                      45.646                      36.802                      30.457                      22.863                      15.269                      7.674                      0.079552 Min</p>
30-10-Step	<p>ANSYS 16.0                      A: Harmonic Response                      Total Deformation - 20000 Hz                      Type: Total Deformation                      Frequency: 20000 Hz                      Sweeping Phase: 0.°                      Unit: mm                      5/11/2020 3:49 AM                      0.11933 Max                      0.10637                      0.09441                      0.083452                      0.073494                      0.064336                      0.055178                      0.046962                      0.039662                      0.033362                      0.027946 Min</p>	<p>ANSYS 16.0                      A: Harmonic Response                      Equivalent (von-Mises) Stress - 20000 Hz                      Type: Equivalent (von-Mises) Stress                      Frequency: 20000 Hz                      Sweeping Phase: 0.°                      Unit: MPa                      5/11/2020 3:50 AM                      323.21 Max                      287.33                      251.44                      215.56                      179.68                      143.79                      107.91                      72.02                      36.138                      0.25303 Min</p>
30-10-Cyl+Exp-5050	<p>ANSYS 16.0                      C: Harmonic Response(5050)                      Total Deformation                      Type: Total Deformation                      Frequency: 20000 Hz                      Sweeping Phase: 0.°                      Unit: mm                      5/6/2020 9:06 PM                      0.021859 Max                      0.019507                      0.017156                      0.014805                      0.012454                      0.010103                      0.0077517                      0.0054005                      0.0030494                      0.00069823 Min</p>	<p>ANSYS 16.0                      C: Harmonic Response(5050)                      Equivalent Stress                      Type: Equivalent (von-Mises) Stress                      Frequency: 20000 Hz                      Sweeping Phase: 0.°                      Unit: MPa                      5/6/2020 9:07 PM                      30.452 Max                      27.003                      23.713                      20.344                      16.874                      13.405                      10.035                      6.6656                      3.2961                      0.12654 Min</p>



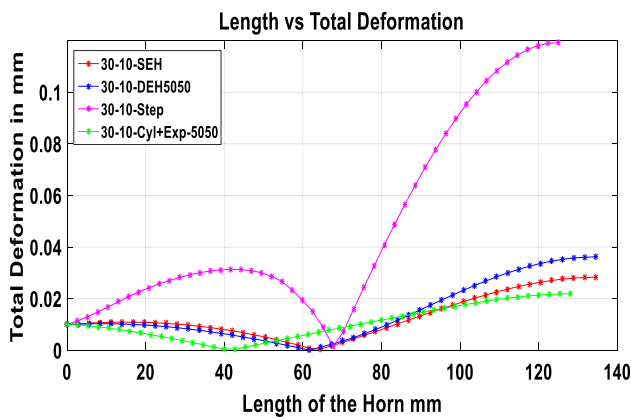


Fig. 12 Variation of deformation along the length for different horn profiles with same diameter ratio

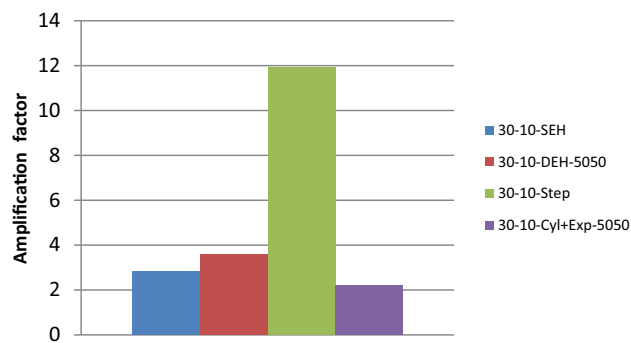


Fig. 13 Variation of amplification for different horn profiles with same diameter ratio

More uniform variation of stress is observed at high tool end diameters along the horn length.

1. Variation in profile revealed higher amplification for stepped horn. At same tool end diameter and length variation, not much variation is observed in terms of deformation and amplification for SEH, DEH as well as mixed profiles. However stresses are higher in stepped profiles.

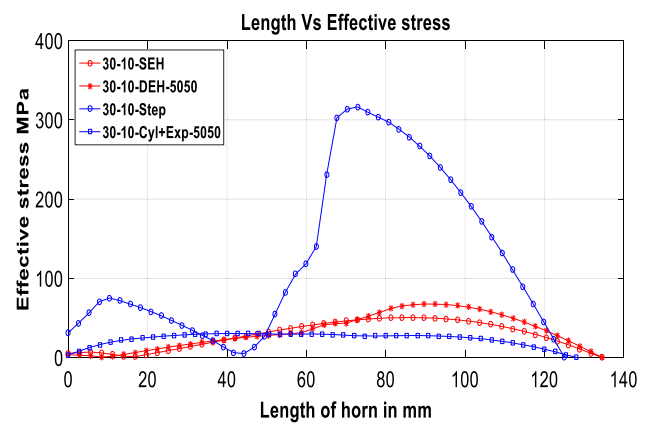
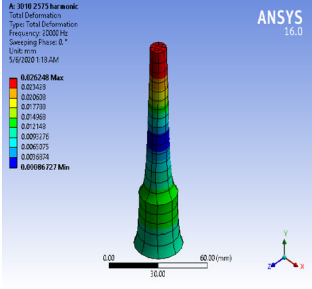
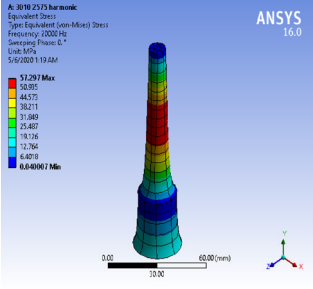
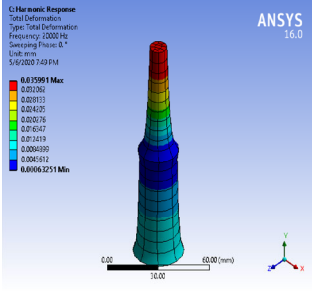
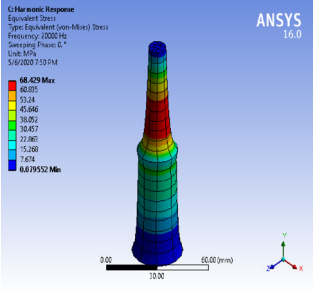
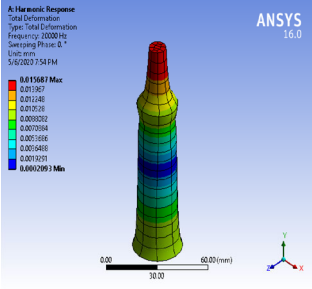
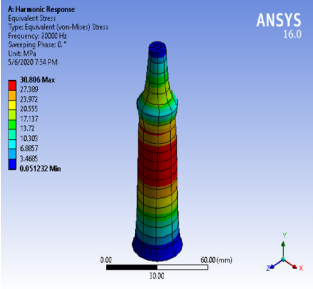
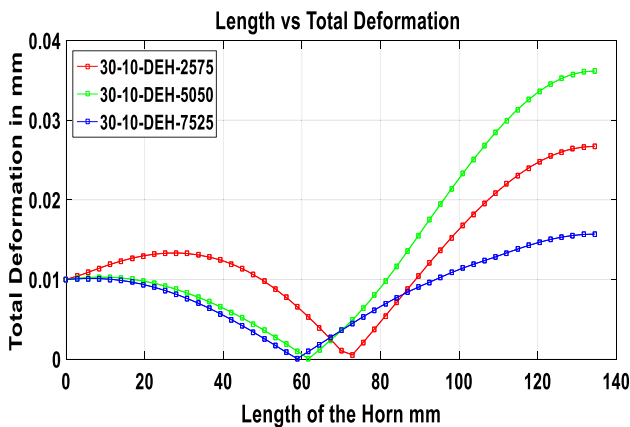


Fig. 14 Variation of effective stress along the length for different horn profiles with same diameter ratio

2. Length variation is also studied at constant diameter ratio with DEH profile. It was concluded that length variation with larger portion of greater diameter, i.e., DEH-7525 is having lower stress than other variations. But the amplification is more in DEH-2575 followed by DEH-5050.
3. Mixed horn profiles are also studied. From the simulation study, it was identified that variation in profile and length variation has no significant effect on the amplification of mixed profile horns whereas diameter ratio is found to be effective. However mixed profiles occupying higher cylindrical portion are subjected to lower stresses.
4. From the overall analysis, it was clear that 30–10-DEH-5050 and 30–10-Cyl + Exp-2575 are having higher amplification other than 30–10-Stepped horn.
5. The stresses are also high in 30–10-DEH-5050 and 30–10-Cyl + Exp-2575 but well below the endurance limit of the horn material, i.e., Ti alloy. For 30–10-Stepped horn though the amplification is high, the stresses are also very high. Hence 30–10-DEH-5050 and 30–10-Cyl + Exp-2575 are chosen as a better designs compared with others.

**Table 10** Total deformation and effective stress variation in DEH with different length variations with same diameter ratio

Diameter ratio D-d	Profile	Total Deformation	Effective stress
30-10	DEH-2575		
	DEH-5050		
	DEH-7525		



**Fig. 15** Variation of deformation along the length in DEH with different length variations with same diameter ratio

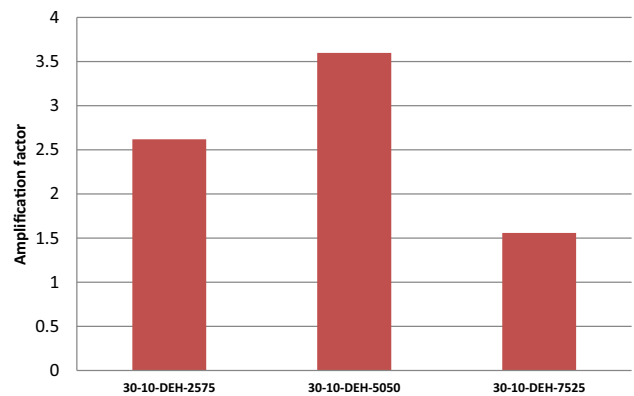


**Fig. 16** Variation of amplification in DEH with different length variations with same diameter ratio

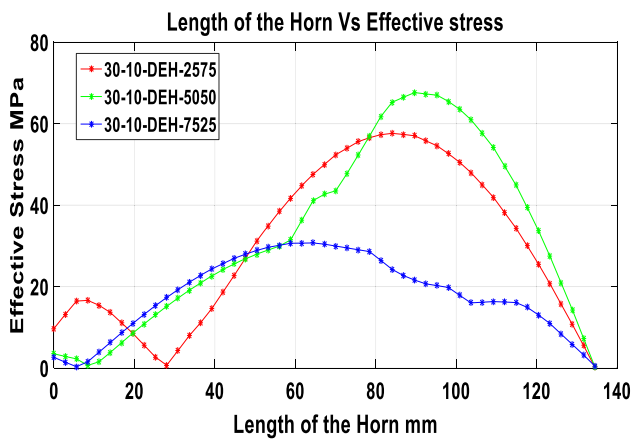


Fig. 17 Variation of effective stress along the length in DEH with different length variations with same diameter ratio

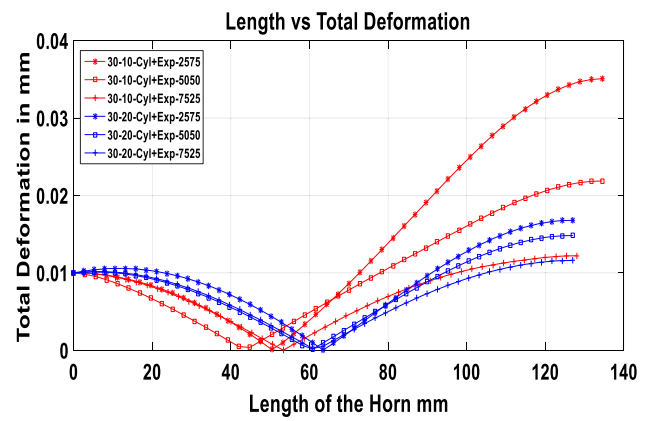


Fig. 19 Variation of total deformation along the length in mixed horn profiles

6. The increment in deformation at lower tool end diameter of horns is attributed to the decreased strength of the horn due to reduced cross sectional area. This offers less resis-

tance to the energy applied causing higher deformation. In addition, sudden changes in the cross section results in stress concentration.

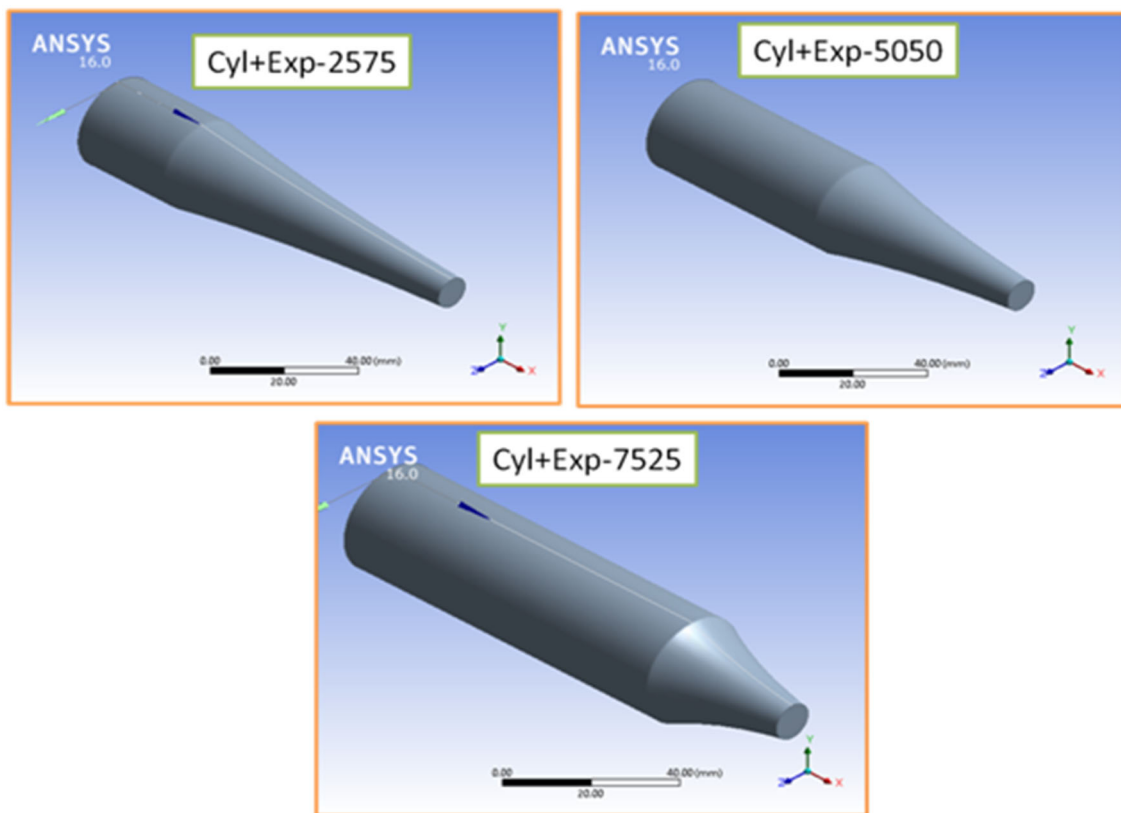
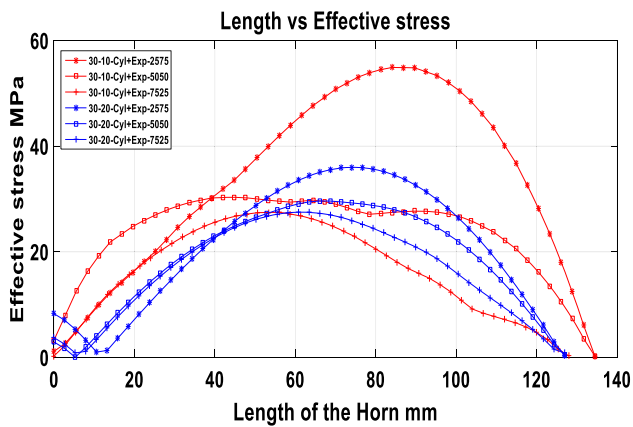
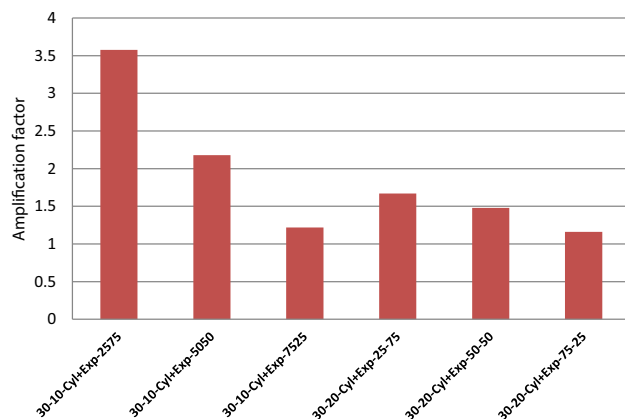


Fig. 18 Mixed horn profiles



**Fig. 20** Variation of effective stress along the length in mixed horn profiles



**Fig. 21** Variation of amplification in mixed horn profiles

## Declarations

**Conflict of interest** On behalf of all authors, the corresponding author states that there is no conflict of interest.

## References

- Amin SG, Youssef HA (1995) Computer-aided design of acoustic horns for ultrasonic machining using finite-element analysis. *J Mater Process Technol* 55:254–260
- Brehl DE, Dow TA (2008) Review of vibration-assisted machining. *Precis Eng* 32(3):153–172. <https://doi.org/10.1016/j.precisioneng.2007.08.003>
- Chandan GK, Sahoo CK (2021) Numerical analysis on a selection of horn material for the design of cylindrical horn in ultrasonic machining. In: Pandey KM, Misra RD, Patowari PK, Dixit US (eds) *Recent advances in mechanical engineering*. Singapore Singapore, Singapore, pp 127–136
- Chhabra AD, Vinod Kumar R, Vundavilli PR, Surekha B (2016) Design and analysis of higher order exponential horn profiles for ultrasonic machining. *J Manuf Sci Prod* 16(1):13–19. <https://doi.org/10.1515/jmsp-2015-0012>
- Chu NH, Ngo QH, Nguyen VD (2018) A step-by-step design of vibratory apparatus for ultrasonic-assisted drilling. *Int J Adv Eng Res Appl* 4:139–148
- Halim NFHA, Ascroft H, Barnes S (2017) Analysis of Tool wear, cutting force, surface roughness and machining temperature during finishing operation of Ultrasonic Assisted Milling (UAM) of Carbon Fibre Reinforced Plastic (CFRP). *Proc Eng* 184:185–191. <https://doi.org/10.1016/j.proeng.2017.04.084>
- He T, Ye XQ, Zhao Y (2015) Optimization design for ultrasonic horn with large amplitude based on genetic algorithm. *J Vibroeng* 17(3):1157–1168
- Jagadish, & Ray, A. (2018) Design and performance analysis of ultrasonic horn with a longitudinally changing rectangular cross section for USM using finite element analysis. *J Braz Soc Mech Sci Eng* 40(7):1–11. <https://doi.org/10.1007/s40430-018-1281-7>
- Kaul S, Joshi T, Gope PC (2018) Design and analysis of sonotrode for ultrasonic eye-punching process. *Int J Mech Eng Technol* 9(9):1276–1283
- Kumar Patel L, Kumar Singh A, Sharma V, Kala P (2020) Analysis of a hybrid ultrasonic horn profile using finite element analysis. *Mater Today Proc* 41:772–779. <https://doi.org/10.1016/j.matpr.2020.08.465>
- Lian H, Guo Z, Huang Z, Tang Y, Song J (2013) Experimental research of Al6061 on ultrasonic vibration assisted micro-milling. *Procedia CIRP* 6:561–564. <https://doi.org/10.1016/j.procir.2013.03.056>
- Llanos I, Campa Á, Iturbe A, Arrazola PJ, Zelaeta O (2018) Experimental analysis of cutting force reduction during ultrasonic assisted turning of Ti6Al4V. *Procedia-CIRP* 77(Hpc):86–89. <https://doi.org/10.1016/j.procir.2018.08.227>
- Moghaddas MA, Short MA, Wiley NR, Yi AY, Graff KF (2018) Performance of an ultrasonic-assisted drilling module. *Int J Adv Manuf Technol* 94(9–12):3019–3028. <https://doi.org/10.1007/s00170-017-0495-7>
- Nath C, Rahman M (2008) Effect of machining parameters in ultrasonic vibration cutting. *Int J Mach Tools Manuf* 48(9):965–974. <https://doi.org/10.1016/j.ijmactools.2008.01.013>
- Nestler A, Schubert A (2014) Surface properties in ultrasonic vibration assisted turning of particle reinforced aluminium matrix composites. *Proc CIRP* 13:125–130. <https://doi.org/10.1016/j.procir.2014.04.022>
- Nguyen HT, Nguyen HD, Uan JY, Wang DA (2014) A nonrational B-spline profiled horn with high displacement amplification for ultrasonic welding. *Ultrasonics* 54(8):2063–2071. <https://doi.org/10.1016/j.ultras.2014.07.003>
- Roopa Rani M, Prakasan K, Rudramoorthy R (2015) Studies on thermo-elastic heating of horns used in ultrasonic plastic welding. *Ultrasonics* 55(1):123–132. <https://doi.org/10.1016/j.ultras.2014.07.005>
- Roy S, Jagadish (2017) Design of a circular hollow ultrasonic horn for USM using finite element analysis. *Int J Adv Manuf Technol* 93(1–4):319–328. <https://doi.org/10.1007/s00170-016-8985-6>
- Satpathy MP, Sahoo SK, Datta S (2016) Acoustic horn design and effects of process parameters on properties of dissimilar ultrasonic welding aluminum to brass. *Mater Manuf Processes* 31(3):283–290. <https://doi.org/10.1080/10426914.2015.1048465>
- Shahid MB, Jung JY, Park DS (2020) Finite element analysis coupled artificial neural network approach to design the longitudinal-torsional mode ultrasonic welding horn. *Int J Adv Manuf Technol* 107(5–6):2731–2743. <https://doi.org/10.1007/s00170-020-05200-5>
- Shakeeb Z, Sarraf A (2019) Design and analysis of ultrasonic horns operating in multiple vibration modes. *J Inf Eng Appl* 2(2):28–32. <https://doi.org/10.7176/jiea/9-3-02>
- Singh DP, Mishra S, Porwal RK (2019) Modal analysis of ultrasonic horn using finite element method. *Mater Today Proc* 18:3617–3623. <https://doi.org/10.1016/j.matpr.2019.07.293>

- Stănăşel I, Buidoş T, Blaga F (2014) Design and fem simulation of ultrasonic welding horn. *Nonconventional Technologies Review/Revista de Tehnologii Neconventionale* 18(1):51–55. Retrieved from [http://www.ultrasonicresonators.org/misc/references/articles/Stanasel\\_'Design\\_and\\_FEM\\_Simulation\\_of\\_Ultrasonic\\_Welding\\_Horn'.pdf](http://www.ultrasonicresonators.org/misc/references/articles/Stanasel_'Design_and_FEM_Simulation_of_Ultrasonic_Welding_Horn'.pdf). Accessed 05 Feb 2020
- Sui H, Zhang L, Wang S, Gu Z (2021) Theoretical and experimental investigation into the machining performance in axial ultrasonic vibration-assisted cutting of Ti6Al4V. *Int J Adv Manuf Technol* 116(1–2):449–472. <https://doi.org/10.1007/s00170-021-07447-y>
- Tadvi M, Prajapati J, Pandey A, Shah J (2015) Design and development of sonotrode for ultrasonic drilling. In: ASME International Mechanical Engineering Congress and Exposition, Proceedings (IMECE), 2B-2015 (August 2016). <https://doi.org/10.1115/IMECE2015-53023>
- Verma, G. C., & Pandey, P. M. (2019). Machining forces in ultrasonic-vibration assisted end milling. *Ultrasonics*, 94(June 2017), 350–363. <https://doi.org/10.1016/j.ultras.2018.07.004>
- Vivekananda K, Arka GN, Sahoo SK (2014) Design and analysis of ultrasonic vibratory tool (UVT) using FEM, and experimental study on Ultrasonic Vibration-assisted turning (UAT). *Procedia Engineering* 97:1178–1186. <https://doi.org/10.1016/j.proeng.2014.12.396>
- Wang DA, Nguyen HD (2014) A planar Bézier profiled horn for reducing penetration force in ultrasonic cutting. *Ultrasonics* 54(1):375–384. <https://doi.org/10.1016/j.ultras.2013.05.002>
- Wang P, Wang D (2020) Evaluation of different tool geometries in the finite element simulation of ultrasonic-assisted drilling of Ti6Al4V. *J Braz Soc Mech Sci Eng* 42(4):1–14. <https://doi.org/10.1007/s40430-020-2266-x>
- Wei L, Wang D (2019) Comparative study on drilling effect between conventional drilling and ultrasonic-assisted drilling of Ti-6Al-4V/Al2024-T351 laminated material. *Int J Adv Manuf Technol* 103(1–4):141–152. <https://doi.org/10.1007/s00170-019-03507-6>
- Xiang D, Shi Z, Feng H, Wu B, Zhang Z, Chen Y, Zhao B (2019) Finite element analysis of ultrasonic assisted milling of SiCp/Al composites. *Int J Adv Manuf Technol* 105(7–8):3477–3488. <https://doi.org/10.1007/s00170-019-04542-z>
- Youssef HA, El-Hofy H (2008) Machining technology: Machine tools and operations. In: *Machining technology: machine tools and operations*. <https://doi.org/10.5860/choice.46-0911>
- Zhao JT, Ning LP, Jiang ZM, Li YL (2021) Design and finite element analysis of longitudinal vibrating stepped ultrasonic horn. *J Phys Conf Ser* 2029(1):012056. <https://doi.org/10.1088/1742-6596/2029/1/012056>

**Publisher's Note** Springer Nature remains neutral with regard to jurisdictional claims in published maps and institutional affiliations.